The structure and control strategies of hybrid solid gravity energy storage system

Wenxuan Tong[1,2], Zhengang Lu[2,3,*], Haisen Zhao[1], Minxiao Han[1], Guoliang Zhao[2], Julian David Hunt[4]

[1] School of Electrical and Electronic Engineering, North China Electric Power University, 102206, China.

[2] State Key Laboratory of Advanced Power Transmission Technology, State Grid Smart Grid Research Institute Co., Ltd., 102209, China.

[3] School of Electrical Engineering, Xi'an Jiaotong University, 710049, China.

[4] International Institute of Applied Systems Analysis (IIASA), Austria

Abstract

Hybrid energy storage is an interesting trend in energy storage technology. In this paper, we propose a hybrid solid gravity energy storage system (HGES), which realizes the complementary advantages of energy-based energy storage (gravity energy storage) and power-based energy storage (e.g., supercapacitor) and has a promising future application. First, we investigate various possible system structure schemes for the proposed HGES. In particular, we also obtained two superior system structure approaches through comparative analysis for two typical application scenarios, distribution and transmission grids. Subsequently, we theoretically analyze and mathematically model the energy conversion relationship of HGES based on different subsystems. More specifically, we discuss the control strategies of HGES in detail at three levels: power electronics, single-type energy storage system, and hybrid energy storage system. In addition, we propose complementary capacity configuration schemes for power-based energy storage systems based on the control strategies. Finally, the proposed HGES structures, control strategies, and capacity configuration schemes for distribution and transmission grid scale are simulated and verified based on MATLAB/Simulink. The results show that the proposed hybrid energy storage system has the advantages of both energy-based and power-based energy storage, which significantly improved compared to single energy storage technologies.

Keywords: Hybrid Energy Storage; Gravity Energy Storage; Power-Based Energy Storage; Control Strategies; System Structure

1 Introduction

In order to fight global warming, more and more renewable energy sources are connected to the power grid to reduce the use of traditional fossil energy. However, wind and solar energy depend on natural factors and cannot be controlled by humans. Consequently, the imbalance between power supply and demand poses a significant challenge to the stable operation of power systems[1-3].

The traditional power system includes five major segments: power generation, transmission, distribution, transformation, and consumption[4, 5]. The supply and demand of electric energy must ensure real-time balance. Applying energy storage in the new power system changes the power system

*Corresponding author

Email address: 13811934901@qq.com (Zhengang Lu)

from a stiff system to a flexible system, with greater flexibility, which is necessary for large-scale renewable energy access[3, 6-8].

According to the energy form, energy storage technology can be divided into mechanical, electrical, electrochemical, chemical, and thermal energy storage[9]. Further, mechanical energy storage, chemical energy storage, and thermal energy storage have the characteristics of large-rated capacity and can be classified as energy-based energy storage technology. On the other hand, electric and electrochemical energy storage has high-rated power and can therefore be classified as power-based energy storage technology, as shown in Fig. 1[10].

Given that different types of energy storage technologies have different characteristics, hybrid energy storage technology combines different energy storage technologies (especially the combination of energy-based and power-based technologies) to achieve technical complementarity, effectively solving the technical problems caused by the only use of a single energy storage technology[7, 11, 12]. Considering that a lack of research has systematically investigated the system structure and control strategies of hybrid gravity energy storage, we conducted the research in this paper.

In the second part of this paper, we combine gravity energy storage (energy-based energy storage, hereinafter referred to as GES) and power-based energy storage, then propose a power-based hybrid gravity energy storage system (PBHSGES, after this referred to as HGES). We discuss various possible structures of the hybrid system and obtain a system structure suitable for two typical application scenarios: distribution and transmission grids. Then the third part quantitatively analyzes the energy flow characteristics in the system. In the fourth part, the control strategies of the power electronics in the HGES, including the machine side inverter, the grid side inverter, and the DC/DC converter, are investigated at the device level, and the coordination of the control is also discussed. In the fifth part, focusing on the single energy storage system level, the power-based energy storage in the hybrid gravity storage system is studied, and three control strategies and their capacity configuration schemes are proposed. The sixth part discusses the overall control scheme from the hybrid energy storage system level. Finally, the proposed system structure approach, control strategies, and capacity configuration schemes for two typical application scenarios (distribution and transmission grids) are simulated and verified based on MATLAB/Simulink.

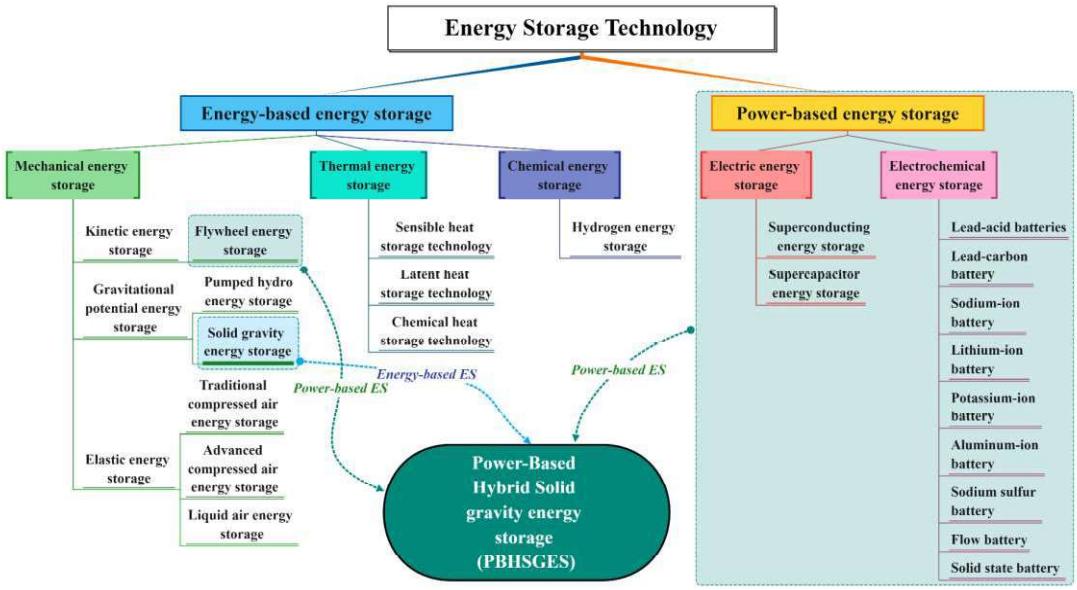

Fig. 1. Relationship between different energy storage technologies and hybrid gravity energy storage

2 System structure of HGES

This chapter first introduces a new energy-based energy storage technology, solid gravity energy storage, then gives the basic composition of the HGES, and finally quantifies the energy conversion relationship of the proposed hybrid system.

2.1. Introduction of solid gravity energy storage

The current energy storage technologies that can be applied on a large scale include pumped storage, battery storage, and compressed air storage. Pumped storage has a long construction period, high cost is limited by geography and water resources, and cannot meet the needs of the rapid development of renewable energy[13, 14]. Battery energy storage can be used in large-scale scenarios, resulting in a complex control system that can reduce operational reliability and pose significant safety risks[15-18]. The cycle efficiency of conventional compressed air energy storage is limited to less than 70% and requires fossil fuels due to the inherent loss of the volume change of the gas[19-21].

GES technology is a forward-looking technology for achieving large-scale clean energy storage, which has been honored by the World Economic Forum as one of the 2020 Technology Pioneers for its high safety and reliability (similar principle to pumped storage), environmental friendliness (no harmful chemical materials and no damage to the natural environment), and high sustainability of energy storage[9, 22, 23].

Both gravity storage and pumped storage are typical energy-based energy storage technologies that achieve large-scale electricity storage through conversion between electrical energy and gravitational potential energy. The storage medium of pumped storage is water, which can achieve stable power output by using continuous water flow to push the turbine. The storage medium of GES technology is modular and discrete weights, which causes the motor to repeatedly start and stop, resulting in a significant loss and noticeable output power fluctuation. Therefore, it reduces the GES system's cycle efficiency and is unsuitable for the power grid's stable operation.

GES technology is still in the early stage of development. The literature [9] has reviewed GES technology and summarized eight types of current GES technology, as shown in Fig. 2, readers interested in this can refer to the literature [9] and [10]. Abstracting various technical routes of GES, the essential operation principle of GES can be obtained: when the electric power of the power system is in excess, the GES system absorbs the electricity through the motor and lifts the weight; when the electric power of the power system is insufficient, the GES system puts down the weight and drives the motor to send out the electricity, which is fed back to the power system[24-31].

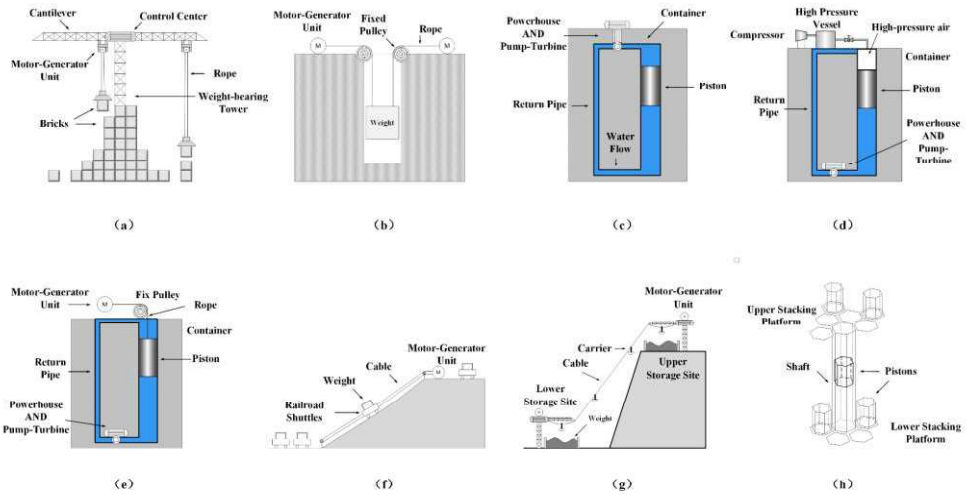

Fig. 2. Schematic diagram of a typical gravity energy storage technology route [10]

2.2. *The basic structure of HGES*

This paper combines GES and power-based energy storage to solve the technical problems of GES technology in the prior art, where repeated starting and stopping of the motor tends to cause large losses and also leads to significant fluctuations in output power.

The basic structure of HGES includes a GES module and a power-based energy storage module, as shown in Fig. 3. The GES unit, as energy-based energy storage, provides a large enough storage capacity for absorbing excess power from the grid or releasing power when the grid power is insufficient. The power-based energy storage module can be composed of any of the power-based energy storage technologies in Fig. 1, whose primary role is to provide a sufficiently large rated power for compensate the fluctuating amount of active power during the operation of the GES device mentioned or to provide fast power support to the grid at the millisecond scale or above.

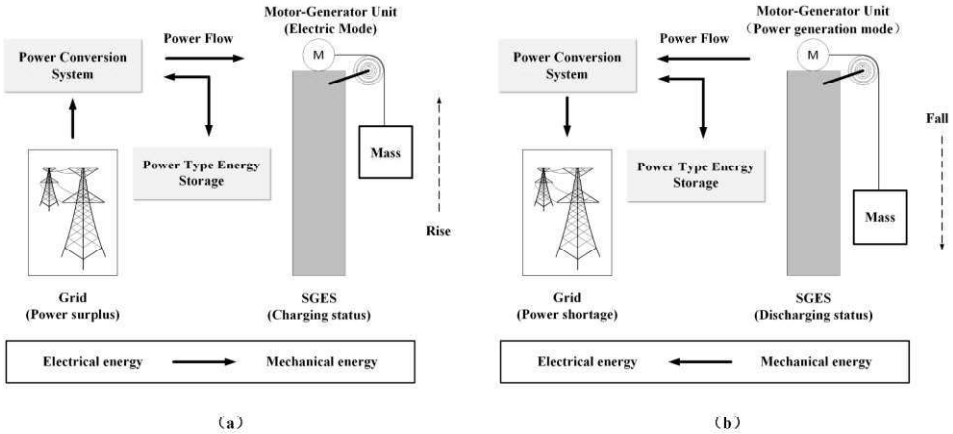

Fig. 3. Schematic diagram of the basic structure and operation principle of HGES

2.3. *Types of HGES*

According to the type of motor, the electric drive equipment, the grid access method, the power-based energy storage access position, and the approach, the HGES has diverse structural composition, as shown in Fig. 4.

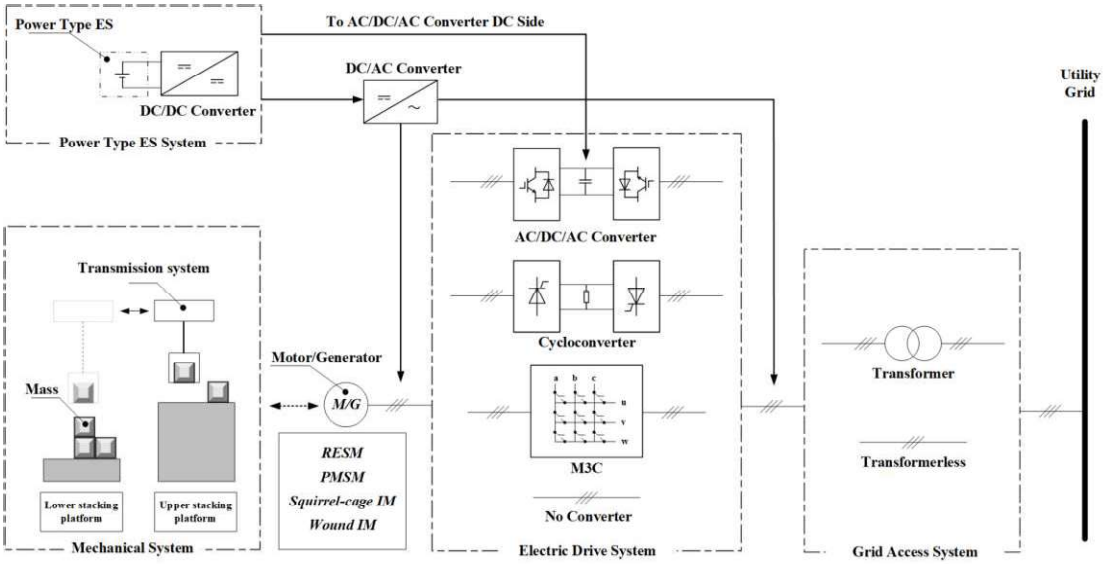

Fig. 4. Different structural solutions for HGES systems

AC motors can be divided into synchronous motors, which include rotor excited synchronous motors (RESM) and permanent magnet synchronous motors (PMSG), and asynchronous motors (induction motors, IM), which include squirrel-cage asynchronous motors (Squirrel-cage IM) and wound asynchronous motors (Wound IM). From a practical aspect, asynchronous motors are by far the most mature and widely used motors. Pumped storage, for example, is the most similar energy storage technology to gravity storage, and asynchronous motors are used in 84.3% of large pumped storage projects[32]. From the economic point of view, the asynchronous motor is cheaper than the synchronous motor, which matches the advantage of the low cost of GES. Therefore, asynchronous motors are attractive for the gravity storage motor segment.

In the electrical drive system part, four possible options include no inverter, Cycloconverter (direct AC/AC converter), matrix converter (M3C), and AC-DC-AC converter (indirect AC/AC converter). Although the Cycloconverter was initially used extensively in variable-speed pumped storage power plants in Japan, it has been phased out due to the advantages of the AD-DC-AD inverter and is only used in a small number of large-scale applications[32-34]. M3C is more suitable for offshore wind power stations and other occupation-sensitive large-scale application scenarios (more than tens of MW), but the current control technology is not yet mature[35-37]. Therefore, the electrical drive section can consider using an AC-DC-AC inverter for motor control or no inverter to simplify the equipment.

For grid access systems, the possible options are direct access to the grid and access to the grid via transformers, which can be discussed for two typical application scenarios: distribution and transmission grids. Direct connection to the grid can be considered for lower voltage distribution grids, thus avoiding the additional investment and losses caused by transformers. When a higher voltage transmission grid is required, a transformer should be considered to provide the required supply voltage for the motor. Regarding the electrical drive system, if the electrical drive system uses inverters, it is possible to connect the grid access system to a lower voltage grid without using transformers. Therefore, the grid access system should consider the voltage level that needs to be connected and the structural configuration of the electrical drive system.

There are three types of approaches for accessing the power-based storage system: accessing it as the front stage of the electrical drive system, accessing it as the backstage of the electrical drive system,

and accessing into the electrical drive system (only if the electrical drive system is feasible with an AD-DC-AD inverter). The first two access strategies require a DC/DC converter for primary power storage control and an additional inverter as the electrical interface, which adds additional investment without significant performance improvement compared to the third access strategy. In contrast, direct access to the electrical drive system improves system reliability and reduces costs, making it a worthy option for power storage access strategies. On the other hand, adopting the direct access strategy also increases the attractiveness of the AD-DC-AD inverter in the electrical drive system.

In summary, in the distribution grid scenario, where the voltage level is low and the system capacity is relatively small given the same current limit, it is oriented to the small-scale application scenario of energy storage. Relevant studies have shown that GES is not economical in small-scale scenarios[38, 39]. Therefore, priority should be given to reducing the system cost. Considering the voltage level in the distribution grid is lower and investment, the direct access strategy should be considered for both the electrical drive system and the grid access system; in addition, to ensure system reliability, the motor should be a wound asynchronous motor. Hence, the power storage can only be connected to the grid using an inverter, and the usage of this part should be combined with the actual demand for technical and economic evaluation.

In the transmission grid scenario, the higher voltage levels and the larger system capacity provide greater room for large-scale energy storage technology. Considering the additional losses caused by transformers (which will be more obvious in large-scale scenarios) and investments, AD-DC-AD inverter could be employed in transmission grids when voltage levels are relatively low (below 3kV, considering the current voltage-withstand level of power electronics). Neutral point clamped (NPC) or fly-across capacitor (FC) topologies in higher voltage-level scenarios. Furthermore, for high-voltage, the modular multilevel topology (MMC) or cascaded full-bridge topology (CHB) can be considered for the transmission grid. In addition, the motor module can use simpler and cheaper squirrel cage asynchronous motors due to an inverter based on fully controlled device. Therefore, for transmission grid scenarios, it is possible to consider configurations that use inverters in the electrical drive system, which avoid using transformers and use squirrel-cage asynchronous motors to reduce costs.

3 Energy flow characteristics of HGES

Generally speaking, the operating state of the energy storage system can be divided into two primary states: charging and discharging. In particular, for HGES, the two primary states of charging and discharging include three sub-states of starting, stable operating, and braking, so there are six basic states of HGES.

From the perspective of system structural composition, HGES can be divided into mechanical systems (including mass modules), motors, electrical drive systems, grid access systems, and power-based energy storage systems. The power flow relationship of each part is shown in Fig. 5.

The power flow of each system in the charging state in Fig. 5 is represented by green arrows; blue arrows represent the power flow in the discharging state; red arrows represent the loss of power flow; the final energy conversion state is represented by yellow; the intermediate energy conversion state is represented by gray, and the lost energy is symbolized by red.

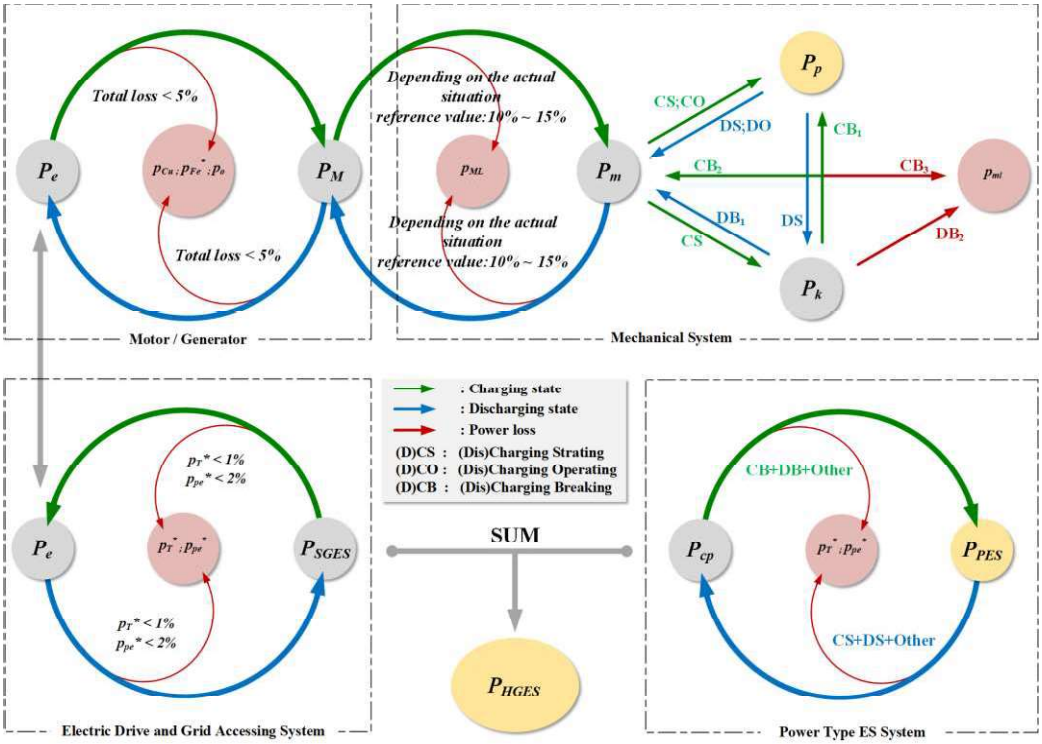

Fig. 5. Energy flow and loss characteristics of the HGES system

3.1. *Energy flow characteristics of Power-based energy storage*

The power of HGES P_{HGES} is synthesized from the fundamental power of the GES system P_{SGES} and the compensating power of the power–based energy storage system P_{cp}.

When the power-based energy storage system absorbs energy during the gravity storage system braking (including charging braking CB and discharging braking DB) and releases energy during the gravity storage system starting (including charging starting CS and discharging starting DS). The energy P_{PES} exchanged by the power-based energy storage is compensated by the power p_T after possible transformer losses p_{pe} and power electronics losses P_{cp}.

In addition, if the power-based energy storage is used for purposes other than compensating GES (e.g., compensating for rapid power fluctuations at the grid side), the model for this part of the power flow is similar.

3.2. *Energy flow characteristics of solid gravity energy storage*

For the GES system, in the charging state, for example, the fundamental power of size P_{SGES} is absorbed from the grid, and the electric power P_e of the motor is obtained after possible transformer losses p_T and power electronics losses p_{pe}. The electric power P_e of the motor is expressed by Eq. (1):

$$P_e = 3U_s I_s cos\varphi_s \tag{1}$$

Where U_s is the motor stator side voltage; I_s is the motor stator side current; $cos\varphi_s$ is the motor stator side power factor.

The electrical power of the motor P_e to the mechanical power of the motor P_M need to consider the internal losses of the motor - including the stator side and rotor copper loss p_{Cu}, iron loss p_{Fe} (permanent magnet motor without this loss) and other stray losses p_o. each variable is expressed by Eq.

(2) to Eq. (4):

$$P_{Cu} = 3I_s^2 R_s + 3I_r^2 R_r \tag{2}$$

$$P_{Fe} = 3I_m^2 R_m \tag{3}$$

$$P_M = T_L \omega \tag{4}$$

Where R_s is the motor stator resistance; I_r is the rotor current which is converted to the motor stator side; R_s is the rotor resistance which is converted to the motor stator side; I_m is the motor excitation current; R_m is motor reluctance; T_L is the motor mechanical torque; ω is the motor mechanical angular velocity.

The mechanical power P_M produced by the motor through the transmission system yields a mechanical loss p_{ML} and finally becomes the power P_m obtained by the mass module. p_{ML} exists because the actual speed of the mass block is low, while the motor speed is high, requiring transmission equipment (such as gearboxes, traction equipment, etc.) for speed matching, and the gearbox ratio K is calculated by Eq. (5):

$$K = \frac{D\omega}{2v_N} \tag{5}$$

Where D is the diameter of the motor; v_N is the rated speed of the mass block.

Based on the conservation of power on both sides of the transmission system, we can obtain the tractive force F by increasing the mechanical torque T_L from the motor after the transmission system:

$$F = \frac{2K}{D} T_L - \frac{p_{ML}}{v_N} \tag{6}$$

Based on the force analysis of the mass module, the following equation can be obtained from Newton's second theorem:

$$F = m(a + g) \tag{7}$$

Based on Eq. (7), the instantaneous acceleration a of the mass block can be calculated as:

$$a = \frac{D}{2K} \frac{d\omega}{dt} \tag{8}$$

The motor's rotor kinematic equation is:

$$\frac{d\omega}{dt} = \frac{\pm T_e \mp T_L - T_0}{J} \tag{9}$$

Where T_e is the electromagnetic torque of the motor, and the positive sign is taken in the electric state; T_0 is the stray resistance torque of the motor, and the negative sign is taken in the electric state.

Combining Eq. (6) with Eq. (9), we can get the mechanical loss p_{ML}:

$$p_{ML} = \frac{2Kv_N}{D} T_L - mv_N \left(\frac{D}{2K} \frac{\pm T_e \mp T_L - T_0}{J} + g \right) \tag{10}$$

Therefore, energy flow analysis in the charging state of the GES system, excluding the mass module, is completed. The analysis of this part in the discharging state is similar.

The power conversion inside the mass module is related to the system's operating state. The following six operating states are discussed in terms of charge start, charge operation, charge brake, discharge start, discharge operation, and discharge brake.

In the charged state, when the mass block rises at a steady speed, all of the mass block power P_m is converted to the mass block gravitational potential energy power P_P. The gravitational potential energy power P_P can be expressed by Eq. (11):

$$P_P = mgv \tag{11}$$

Where m is the mass of the mass block; g is the acceleration of gravity, which is a constant of

247 $9.81\,m/s^2$; v is the instantaneous velocity of the mass module.

248 When in the starting state, the block starts to move from a standstill, so there is a kinetic energy
249 power P_k, and the power of the mass module P_m will be converted into two parts: gravitational potential
250 energy power P_P and kinetic energy power P_k. The kinetic power P_k and the power of the mass
251 module P_m are expressed by equations (12) and (13):

252 $$P_k = mav \tag{12}$$

253 $$P_m = mv(a + g) \tag{13}$$

254 Where a is the instantaneous acceleration of the mass block.

255 When in the braking state, the block gradually changes from running to stationary, so the same
256 kinetic power P_k exists. in contrast to the starting state, the kinetic power P_k is negative at this time,
257 which is reflected in the energy perspective as a gradual reduction of the kinetic energy of the mass block.
258 However, the flow direction of the kinetic power P_k in the braking state is related to the system structure
259 and its control strategy. The possible flows include conversion to gravitational potential power P_P
260 (uncontrolled kinetic strategy), conversion to mass block power P_m for feeding back to the grid (motor
261 feedback braking strategy) or conversion to mass-side loss power P_{ml} (electrical consumption braking
262 or mechanical braking).

263 In the discharged state, when the mass block maintains a steady rate of descent while dragging the
264 motor to generate electricity, all of the mass block's gravitational potential energy power P_P is converted
265 to mass power P_m and generates motor-side mechanical power P_M. When in the starting state, similar
266 to the charge starting state, mass power P_m is converted to kinetic energy power P_k with gravitational
267 potential energy power P_P. When in the braking state, P_k may be converted to mass block power P_m
268 for return to the grid (motor feedback braking strategy) or converted to mass-side loss power P_{ml}
269 (electrical consumption brake or mechanical brake)

270 4 Power electronics control strategies

271 The control of power electronics is at the bottom, and the foundation of the control of HGES, so the
272 control of HGES relies heavily on the control of power electronics. This section focuses on two systems
273 involving power electronics: electrical drive and power-based energy storage systems. Based on the
274 discussion in Section 2.3, this section will discuss the control strategy of power electronics in AC-DC-
275 AC inverter (electrical drive system) and DC/DC converter (power-based energy storage system) based
276 on the perspective of HGES control.

277 *4.1. Motor-side inverter*

278 The motor-side inverter refers to the inverter near the motor side of the AC-DC-AC inverter in the
279 electrical drive system. The control object of the motor-side inverter is the motor, and its control can be
280 divided into scalar control (SC) and vector control (VC). Vector control is the industry's most widely
281 used control technology for high-power drive systems because of its better dynamic response, energy
282 consumption characteristics, and control accuracy.

283 According to flux orientation, vector control can be divided into flux orientation control (FOC)
284 based on rotor flux orientation and direct torque control (DTC) based on stator flux orientation.

285 The basic control model of FOC is shown in Fig. 6. The equivalent DC motor model is obtained by
286 coordinate transformation, and then the torque is controlled by the flux chain component according to
287 the control method of the DC motor. Finally, the resulting control quantities are converted to the

corresponding quantities in the three-phase coordinate system by inverse coordinate transformation for control. In Fig. 6, ASR (Automatic Speed Regulator) is the speed regulator, and AFR (Automatic Flux Regulator) is the flux regulator, and the coordinate transformations involved are as follows:

$$T_{3s/2s} = \sqrt{\frac{2}{3}}\begin{bmatrix} 1 & -\frac{1}{2} & -\frac{1}{2} \\ 0 & \frac{\sqrt{3}}{2} & -\frac{\sqrt{3}}{2} \end{bmatrix} \tag{14}$$

$$T_{2s/2r} = \begin{bmatrix} cos\varphi & sin\varphi \\ -sin\varphi & cos\varphi \end{bmatrix} \tag{15}$$

Suppose the slight delay caused by the power electronics is ignored, and the coordinate transformation and its inversion cancel each other. In that case, the link in the dashed box in Fig. 6 can be omitted and is equivalent to direct control of the equivalent DC motor, thus bringing a dynamic response performance comparable to the DC speed regulation system.

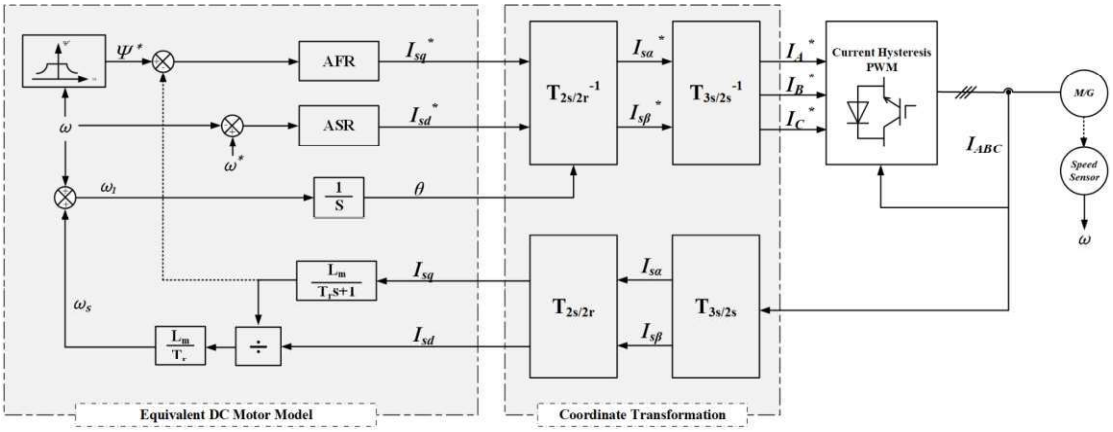

Fig. 6. Control flow chart of FOC control system based on three-phase current hysteresis

Direct torque control (DTC) is another high-performance vector control technology developed after FOC. Unlike the speed-oriented control of FOC, the main feature of DTC is the direct control of motor torque. DTC is based on the orientation of the motor stator flux, and the deviation of the stator flux amplitude from the electromagnetic torque is reduced by selecting the appropriate space voltage vector through SVPWM technology, as shown in Fig. 7.

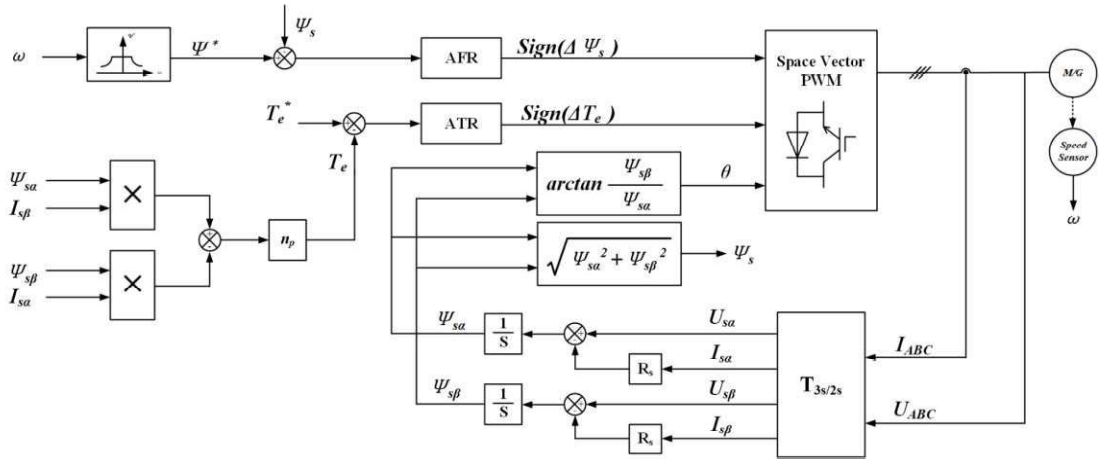

Fig. 7. Control flow chart of SVPWM-based DTC control system

With the development of digital processors, the above two vector control techniques can be implemented in engineering at a low cost, thus becoming the most widely used high-performance motor control techniques. The comparison between FOC and DTC is shown in Table 1, both are based on the dynamic model of the motor, and the torque and flux components of the three-phase stator current are separated through coordinate transformation to achieve decoupled control, which enables the induction motor to achieve dynamic performance comparable to the DC motor.

Stable and reliable control of the mass module during operation is the most basic requirement of the gravity storage system, so it is desired to provide stable torque control over a wide range of speed variations. From the speed regulation and torque control perspective, FOC is more suitable for gravity storage requirements. On the other hand, DTC control requires fewer motor parameters and does not require complex rotational coordinate transformation. Therefore, it still has better control robustness when the motor parameters change, which improves the reliability of the electrical drive system in unconventional conditions.

In summary, FOC is more suitable for achieving high-performance control under stable conditions, while DTC may perform better in the face of fault conditions. We can consider switching different control strategies in different situations to achieve the best-integrated control effect when hardware conditions allow.

Table.1 Comparison of the control characteristics of FOC and DTC [40, 41]

	DTC	FOC
Flux control	Stator flux control	Rotor flux control
Torque control	Multi-position control, larger pulsation	Continuous control, less pulsation
Current control	Uncontrollable	Closed-loop control
Coordinate transformation	Static coordinate transformation	Rotating coordinate transformation
Speed range	Narrower	Wider
Required parameters	R_s	R_s , R_r , L_s , L_r , L_m
Control robustness	Good	Normal
PWM strategy	Hysteresis or SVPWM	Hysteresis or SVPWM

4.2. Grid-side inverter

Grid-connected control is an essential requirement for energy storage systems, and the performance of its grid connection directly affects the overall performance of the energy storage system. The main body of grid-connected control is the grid-side inverter, i.e., the AC-DC-AC inverter near the grid side in the electrical drive system. Generally speaking, the main content of grid-connected control is the control of active and reactive currents, i.e., active power (or node phase angle) and reactive power (or node voltage).

The instantaneous power in the stationary three-phase coordinate system is defined as:

$$P = |V_{abc}||I_{abc}|cos\varphi \tag{16}$$

$$Q = |V_{abc}||I_{abc}|sin\varphi \tag{17}$$

By transforming the above two equations by $T_{3s/2s}$ and $T_{2s/2r}$, we can obtain the instantaneous power expression based on the grid voltage orientation after rotating the coordinate system:

$$P = V_d I_d + V_q I_q \tag{18}$$

$$Q = V_q I_d - V_d I_q \tag{19}$$

When the grid voltage is stable, i.e., V_d is constant, active and reactive power can be controlled by

controlling the dq-axis component of the inverter output current. The DC-side voltage of the AC-DC-AC inverter is related to the power flow at both ends of the dc-side. Assuming that the dc power input at the rectifier side is constant, the dc-side voltage will be controlled by the active power output at the inverter side, so the dq-axis component of the inverter current will be controlled can also achieve the control of the dc-side voltage, as shown in Fig. 8.

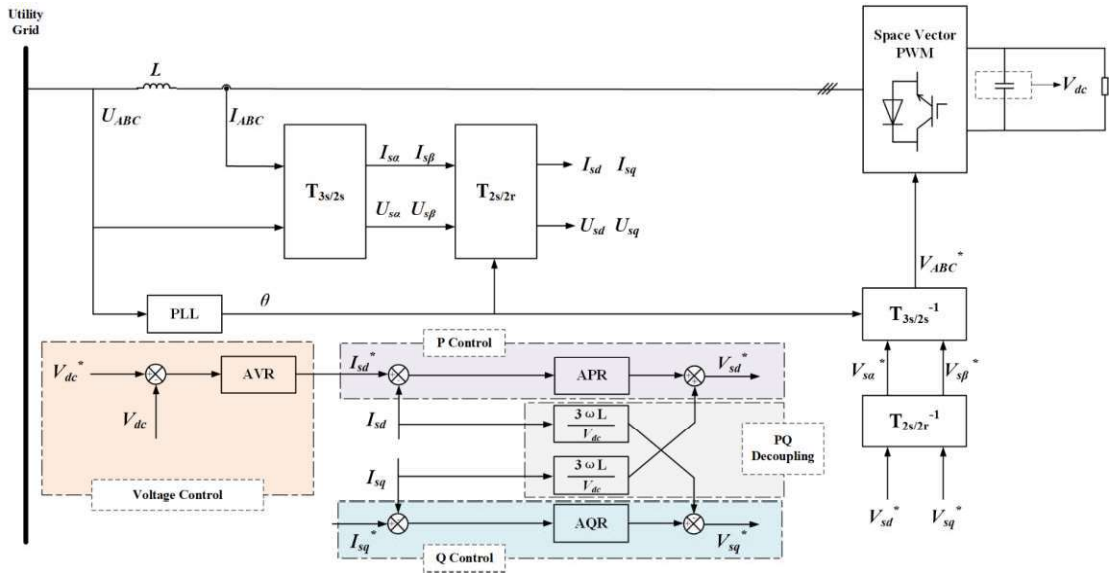

Fig. 8. Control System of Grid-connected Inverter

The control system samples the three-phase voltage and current on the grid side and obtains the phase angle of the voltage through a phase-locked loop (PLL), then uses a coordinate transformation to get the voltage and current vectors in a two-phase rotating coordinate system. The decoupling control loop consists of voltage, active power loop, and reactive power loop, which can be switched to active power control by removing the voltage control part when voltage control is not used. Since the current component of the dq axis is coupled, which makes the decoupling control of PQ complicated, thus feedforward control is introduced for decoupling. The output of the decoupled control loop through the inverse coordinate transformation gets the three-phase voltage reference vector, which SVPWM modulates to generate the three-phase switching signal to control the grid-connected inverter.

4.3. DC/DC converter

The function of the DC/DC converter is to convert DC power from one voltage level to another voltage level, playing a role similar to the DC transformer. For a hybrid GES system, even at the lowest 380 V distribution voltage level, if an AC-DC-AC converter is used as the electrical drive system, the bus voltage on its DC side will be above 560 V. On the other hand, the supercapacitor, as a typical and mature power-based energy storage device, the rated voltage of a single unit is only 2.7 V[42-44]. If DC/DC converter is not used for voltage matching, a large number of devices will be connected in series, which is undesirable in terms of economy and technology.

The control system of the DC/DC converter is shown in Fig. 9. The DC/DC converter suitable for the energy storage system requires control of the energy flow in both directions, so a Boost/Buck bidirectional converter is used. In order to provide sufficient voltage, the power-based energy storage side still needs some devices connected in series. The control part is similar to the control of the grid-side inverter, including voltage control and power control, and again, the voltage control part is not added

when power control is used.

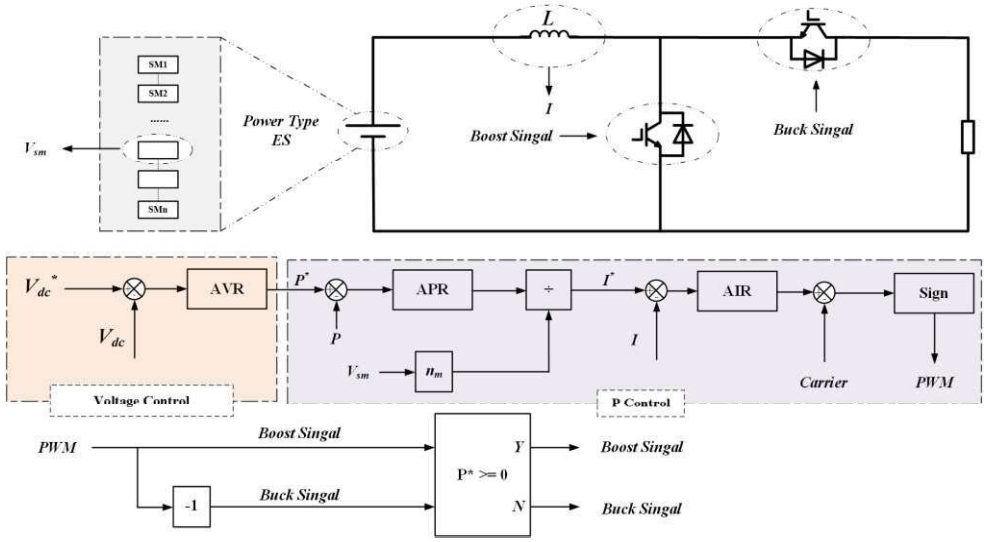

Fig. 9. DC/DC converter control system

4.4. Discussion on control coordination

Based on the discussion in Section 2.3, in the distribution grid application scenario, a wound asynchronous motor can be directly connected to the grid, where the gravity storage part does not involve power electronics, and there is no control problem at the power electronics level. Power-based energy storage devices are connected to the grid through DC/DC converters and inverters, which can be designated for power control and DC bus voltage control, respectively.

In the transmission grid scenario, the AC-DC-AC inverter-based configuration has many advantages, including significantly reducing the number of grid-side inverters through a shared DC bus strategy, as shown in Fig. 10.

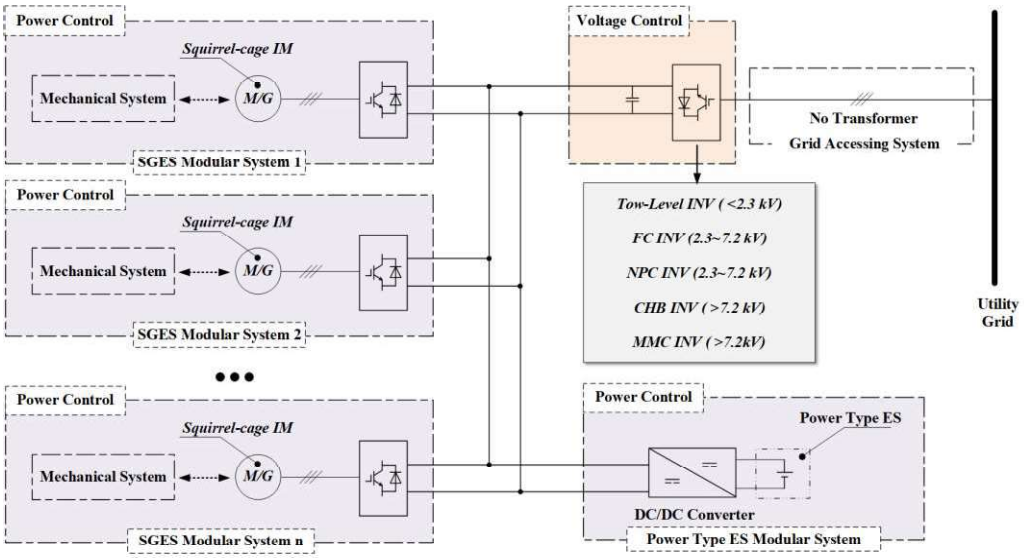

Fig. 10. Schematic diagram of HGES at the transmission grid level

When a common DC busbar strategy is used, additional devices for gravity and power-based energy storage can be connected to the system with a minimum number of power electronics, improving the cost and reliability of the system significantly. The DC-side bus will be expanded into a micro DC network,

facilitating the connection of other possible DC devices (such as PV arrays). On the other hand, with DC-side structures becoming complex, connected power electronics will face control coordination problems.

The primary node types of AC-based power systems include PQ, PV, and Vθ nodes. The PQ node is a node where the amounts of active and reactive power exchanges are determined. The PV node has some reactive power compensation capability to ensure its node voltage is stable. The Vθ node is also called a balancing node, which has a large capacity and can ensure the power balance of the whole grid, and this node is both necessary and unique based on the consideration of control stability.

In analogy with the node characteristics of the AC grid and considering that there is no reactive power in the DC grid, it is easy to find that the DC microgrid should include two types of nodes, P-node and V node, corresponding to the power control and voltage control in the aforementioned power electronic control strategy. From the control aspect, several P nodes can be under the DC grid to ensure the stability of node exchange power through power control; V nodes should still exist and be unique for ensuring the voltage stability of the whole DC grid. Considering the V node based on the power perspective, the sufficient and necessary condition to maintain the DC voltage stability should be that the node can complete the power balance of the whole network, so the V node must have sufficient capacity.

Considering that the grid-side inverter can exchange power between the entire DC microgrid and the AC main grid, it is inevitable that it will have the largest equipment capacity in the whole DC microgrid. So we can set the grid-side inverter as the V node, as shown in Fig. 10. Another advantage of this control strategy is that since a larger capacity of the grid-side inverter is required, a modular multilevel topology is more likely to be used to facilitate access to higher voltage transmission grids, which will avoid the potential use of transformers (thus reducing investment and losses).

5 Compensation and configuration strategy of Power-based ES

For a GES system with a certain capacity, the HGES needs to be configured with the corresponding capacity of power-based energy storage, which will affect the overall economy of the system. If the configured capacity is too large, it will affect the economic performance of the hybrid system. While the configured capacity is too small, the technical performance will deteriorate, so it is necessary to determine the appropriate capacity configuration scheme for power-based energy storage. The capacity configuration scheme of power-based energy storage is related to the compensation strategy for a given demand, so various capacity configuration schemes in this chapter will be presented based on different compensation strategies.

According to Eq. (9), when driving a constant torque load, the way to change the motor speed (i.e., the mass module movement state) is to change the electromagnetic torque of the motor. Simplifying the actual GES as a first-order inertia loop, the response of its tractive force (torque) step command is an exponential function, and let the horizontal segment F_h, rising segment F_{up} and falling segment F_{down} of its tractive force response curve be:

$$F_h = B_2 mg \tag{20}$$

$$F_{up} = B_m mg + (B_n - B_m)mg(1 - e^{-At}) \tag{21}$$

$$F_{down} = B_n mg + (B_m - B_n)mge^{-At} \tag{22}$$

where time $t \geq 0$, B_m is the initial coefficient of traction force, B_n is the final coefficient of traction force, and A is related to the motor, transmission system, and mass block used, reflecting the inertia of the entire gravity energy storage system. To simplify the analysis, we combine the above three

traction forces and considering the gravity of the mass module, the combined external force on the mass module can be expressed uniformly as:

$$F = (B_n - 1)mg + (B_m - B_n)mge^{-At} \tag{23}$$

To simplify the analysis, we assume that three steady-state traction forces exist in this example: $B_1mg > B_2mg = mg > B_3mg$. Therefore, the velocity response curve can be calculated by the following equation:

$$v = v_0 + \int_{t_0}^{t_0+\Delta t} \frac{\Delta F}{m} dt \tag{24}$$

Where, $t_0$is the initial moment of traction force change, Δt is the traction force change elapsed time, taking $t_0 = 0$, the velocity and acceleration response curve can be obtained according to Eq. (23), which is generated by the combined external force F:

$$v = v_0 + (B_n - 1)g\Delta t + (B_m - B_n)\frac{g}{A}(1 - e^{-A\Delta t}) \tag{25}$$

$$a = (B_n - 1)g + (B_m - B_n)ge^{-A\Delta t} \tag{26}$$

In particular, when the traction coefficient satisfies Eq. (27), Eq. (25) and Eq. (26) can be further simplified to Eq. (28) and Eq. (29):

$$\forall |B_m - B_n| = C \tag{27}$$

$$v = v_0 + \frac{Cg}{A}(K_1 A\Delta t + K_2(1 - e^{-A\Delta t})) \tag{28}$$

$$a = Cg(K_1 + K_2 e^{-A\Delta t}) \tag{29}$$

Where C is a constant, $K_1 \in \{1,0,-1\}$, $K_2 \in \{1,0,-1\}$ and $K_1K_2 \neq 1$.

So far, the tractive force and velocity curves of the mass block downward and upward can be plotted schematically, and the exchange power schematic can be plotted according to Eq. (30):

$$P = Fv \tag{30}$$

The tractive force curve, mass module velocity curve, and exchange power curve are shown on the left side of Fig. 11. Due to the inherent inertial loop of the electromechanical system leads to the existence of nonlinear segments of the curve, among them, the nonlinear situation of the power curve is the most serious. The most unfavorable power nonlinear segment to the system's normal operation is the power spike generated during the start-up phase of gravity storage charging and the discharge braking phase, which will produce overcurrent and voltage instability at the machine if not suppressed.

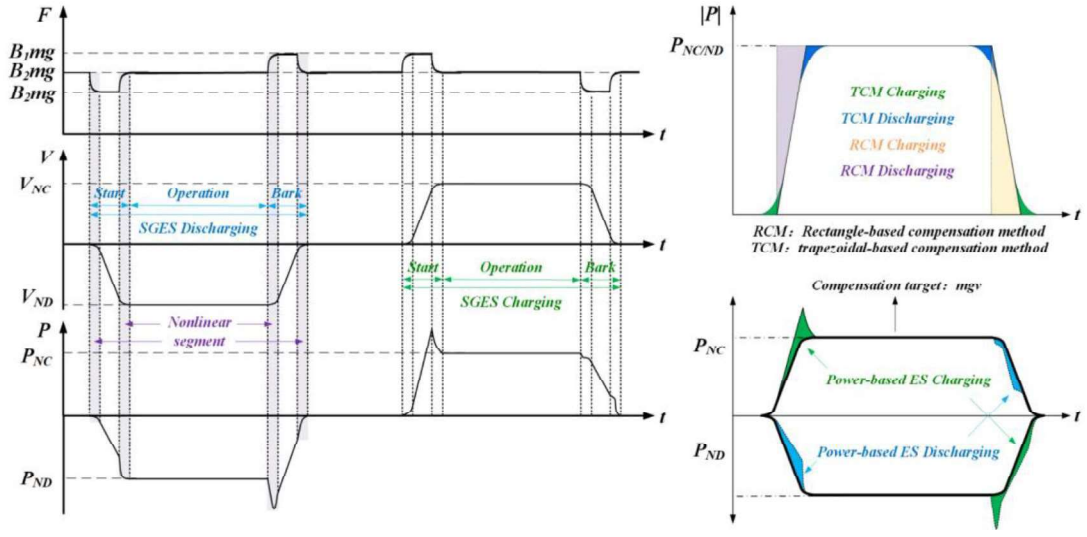

Fig. 11. Power-based energy storage compensation method diagram

Explained from the analytical perspective, based on Eq. (30), it is clear that the nonlinearity is most pronounced since the exchange power curve is the product of the tractive force curve and the velocity curve.

From the energy perspective, based on the discussion in Section 2.4, the kinetic energy stored during the operation of the mass module is released during the charging starting and discharging braking phases. Due to the motor feedback braking strategy (including DTC and FOC), the kinetic energy is fed back to the grid through the DB1 and CB2 paths in Fig. 5, and this energy is stacked on the gravitational potential energy power resulting in a power spike. For the same reason, the exchange power inversion between the charging braking and discharging starting phases can be explained.

Further, based on the power conversion triangle of the mass module in Fig. 5, with Eq. (11)-Eq. (13), we can know that the exchange power is the superposition of gravitational potential energy power and kinetic energy conversion power.

In a single run (rising or falling), gravitational potential energy power has a sign-preserving, more moderate change, while kinetic energy power undergoes a positive and negative change that conforms to the relatively drastic change.

Therefore, if we can remove the kinetic energy power, a more drastic change in the component, we can obtain a more stable exchange power curve. Based on this idea, the compensation method obtained is called the compensation method based on the gravitational potential energy power, as shown in Fig. 11 right below.

The capacity E_1 of the power-based energy storage module to be configured for the gravitational potential power-based compensation method can be obtained from Eq. (31):

$$E_1 = \frac{1}{2} m v_m^2 \eta_M \tag{31}$$

Where v_m is the maximum speed of the mass module operation, η_M is the motor efficiency.

The compensation method based on gravitational potential power suppresses the power spikes and sags brought by kinetic power and reduces the capacity of power transmission equipment. It also facilitates the design of filters because the original irregular exchange power curve becomes regular and symmetrical.

Considering that there are still nonlinear segments in the gravitational potential-based compensation method, a linearized compensation method is further proposed on this basis, including the trapezoidal-based compensation method (TCM) and the rectangle-based compensation method (RCM), as shown in the upper right of Fig. 11.

The linearization-based compensation method makes the overall power external characteristics of the HGES more regular and facilitates the dispatch at the microgrid scale. In particular, the rectangular-based compensation method, based on the trapezoid-based compensation method, improves the full power response time of the HGES from the original motor response time level to the power-based energy storage device response time level, which significantly improves the response speed of the HGES. Because the exchange power response curve of the rectangular-based compensation method is very close to the rectangle when viewed on the original time scale. The method is thus entitled.

Based on Eqs. (12), (13), (28), and (29), the required configuration capacity E_2 of the power-based energy storage module based on the trapezoidal-based compensation method can be expressed as:

$$E_2 = E_1 - (E_{start\ up} - \frac{v_{strat\ up}^2|_{t=\Delta t}}{2a_{up}})\eta_M \tag{32}$$

$$v_{start\ up} = (B_1 - 1)g\left(t + \frac{e^{-At} - 1}{A}\right) \tag{33}$$

$$E_{start\ up} = mg\int_0^{\Delta t} v_{start\ up}\, dt \tag{34}$$

$$a_{up} = (B_1 - 1)g(1 - e^{-At}) \tag{35}$$

where $v_{start\ up}$ is the speed of the mass module in the start-up phase; $E_{start\ up}$ is the energy absorbed by the mass module in the start-up phase; and a_{up} is the acceleration of the mass module in the upward uniform acceleration phase.

The required configuration capacity E_3 of the power-based energy storage module based on the rectangular compensation method can be expressed as the difference between the triangular area in Fig. 11 and the area of the original irregular region:

$$E_3 = \frac{v_m^2}{2a_{up}}\eta_M - E_1 \tag{36}$$

In summary, this chapter investigates the tractive force, velocity, and power of GES's mass modules. The power compensation and capacity configuration strategies of three power-based energy storage are given based on the external characteristics of its exchange power.

The compensation method based on gravitational potential power decouples the exchange power of the mass module, separates the gravitational energy storage power from the kinetic energy power based on the power triangle in Fig. 5, and eliminates the kinetic energy power component that fluctuates significantly to improve the stability and symmetry of the power waveform.

The trapezoid-based compensation method achieves the complete linearization of the external characteristics of the power. On this basis, the rectangular-based compensation method is further induced to improve the full power response time from the GES system to the power-based energy storage response time so that the HGES has both the energy storage capacity of the energy-based energy storage and the response speed of the power-based energy storage.

6 Coordinated control strategies at the hybrid energy storage system level

For two typical application scenarios in transmission and distribution grid, two types of HGES and their control signals are shown in Fig. 12. The distribution grid level HGES is shown in the blue part of Fig. 12, and the transmission grid level hybrid gravity storage system is shown in the green part of Fig. 12.

The two types of HGES are similar in terms of the control process. First, the system state is sampled, including at least three critical parameters: mass module operating speed V, mass module operating position S, and motor speed n. The resulting signals are sent to the logic decision system for system operating state identification to give the corresponding control signals.

The control strategies for the two types of HGES differ due to the system structure; thus, the final output control signals are also varied. The control strategies are introduced according to the six basic operating states of GES.

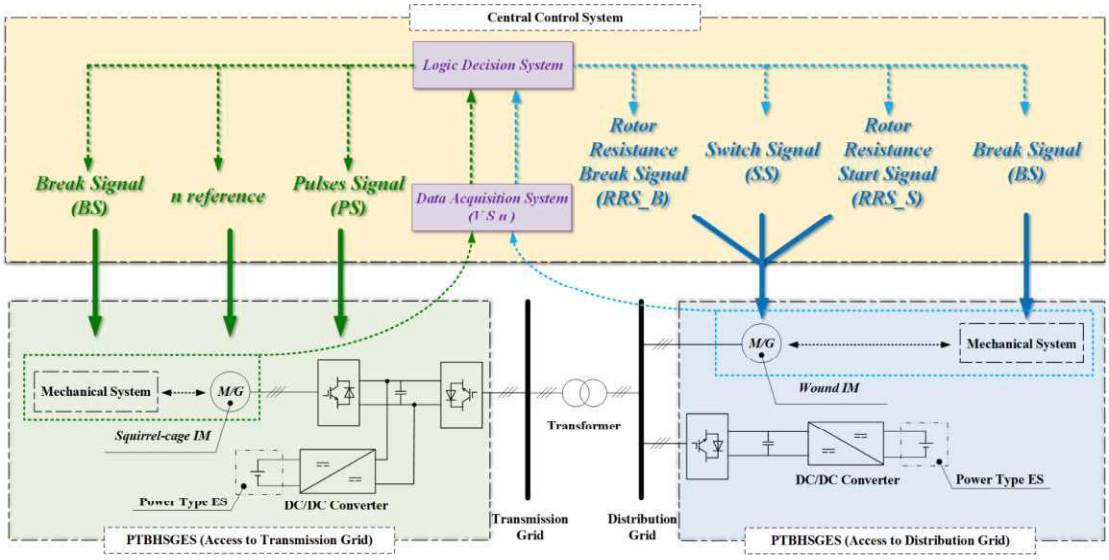

Fig. 12. Hybrid system-level control flow chart of HGES

6.1. Distribution grid-level HGES control strategy

The HGES applied to the distribution grid is shown in the blue part of Fig. 12. Based on the discussion in Section 2.3, the motor is a wound asynchronous motor, and both the electrical drive system and the grid access system use a direct access strategy. Power-based energy storage is controlled by a DC/DC converter for power control, then connected to the distribution grid after the DC-side voltage control by the inverter.

A significant starting torque is required when the system is in a charging starting state because the motor needs to start with a mass module. In order to avoid stalling and to suppress the starting current, a strategy of adding a starting resistor in series with the rotor (which is one of the reasons for not using a squirrel-cage motor) is used, and the starting resistor is removed after sufficient speed is reached to bring the motor into normal operation. We can obtain the value of the starting resistance is obtained through the motor electromagnetic torque equation, and the motor electromagnetic torque after the rotor series resistance can be expressed as:

$$T = \frac{3pU_s^2 \dfrac{R_r + \Delta R_r}{S}}{2\pi f_s \left[\left(R_s + \dfrac{R_r + \Delta R_r}{S}\right)^2 + (X_s + X_r)^2\right]} \tag{37}$$

Where T is the electromagnetic torque; p is the number of motor pole pairs; U_s is the RMS value of the stator-side phase voltage; R_r is the rotor resistance; ΔR_r is the resistance in series with the rotor; f_s is the stator-side frequency; R_s is the stator-side resistance; X_s is the stator-side inductance; X_r is the rotor-side inductance; S is the slip rate. To obtain the maximum starting torque, the required series resistance ΔR_r can be solved by bringing $S = 1$ and $T = T_m$ (T_m is the maximum electromagnetic torque) into Eq. (37).

When the system is in charging operation, the power absorbed by the mass module will be steadily converted to gravitational potential energy power, and the system components are in a steady state without special control.

When the system is in a charging braking state, the motor rotor is strung into the braking resistor for electrical braking to complete the deceleration (if a squirrel cage motor is used, it will face the problem of braking difficulties). When the speed drops to zero (or low enough), the motor brakes and

the braking resistor is removed, and the system is removed from the grid and then leaves the grid. The braking resistance is similar to the starting resistance and can be solved by bringing $S = 1$ and $T = T_L$ (T_L is the load torque) into Eq. (37) to find the required series resistance ΔR_r.

When the system is in a discharged start condition, the same starting resistance is needed as for a charged start, not because the starting torque is insufficient - it should be noted that the driving and drag properties of the electromagnetic torque and the load torque have been exchanged - but to limit the excessive start-up current. In particular, at this point, the mass module will be in a downward process, and the motor will be counter-rotating. In order to keep the motor in a discharged state, it is necessary to connect to a negative sequence three-phase power supply - by exchanging any two phases of the three-phase grid-connected mechanical switch. After reaching enough speed to remove the starting resistance, the system turns into normal operation.

When the system is in the discharging operation state, the gravitational potential power is steadily released as the output power of the mass module, and all parts of the system are in a steady state without special control.

When the system is in the discharging braking state, it is noted that the electromagnetic torque is resistance in nature. If the rotor braking resistor is directly connected to the rotor, the electromagnetic torque will be further reduced, leading to the out-of-control of the mass module (free fall), so the braking resistor should be connected after the positive sequence three-phase power supply is reconnected. After the mass module is stationary, the motor will be held, the braking resistor removed, and the system off-grid. In particular, when the system encounters an unexpected fault and needs to stop in an emergency, the control strategy of discharge braking can also be used.

In conclusion, the control strategy at the distribution grid level can be organized as Table 2 for the logic decision system in Fig. 12. The SS indicates the network side mechanical switching signal, which is 1 when connected to positive sequence three-phase power, 2 when connected to negative sequence three-phase power, and -1 when off-grid; BS indicates the braking signal, which is -1 when not braking (normal operation) and 1 when braking; the rotor series starting and braking resistor signals are RRS_S and RRS_B respectively, which are 1 when connected and -1 when removed.

Table.2 Control logic table for distribution grid-level HGES

System Status	SS	BS	RRS_S	RRS_B
CS ($\|n\| > \|n_s\|$)	1	-1	1→(-1)	-1
CO	1	-1	-1	-1
CB ($V = 0$)	-1	-1→(1)	-1	1→(-1)
DS ($\|n\| > \|n_s\|$)	2	-1	1→(-1)	-1
DO	2	-1	-1	-1
DB ($V = 0$)	1→(-1)	-1→(1)	-1	1→(-1)

6.2. Transmission grid-level HGES control strategy

The HGES applied to the transmission grid is shown in the green part of Fig. 12. Based on the discussion in Section 2.3, the motor is a squirrel-cage asynchronous motor and the electrical drive system is an AC-DC-AC inverter, and the machine side inverter is controlled by the FOC because the FOC is a direct control of the rotational speed, which is more convenient in the control system design. The incoming system adopts the direct access strategy, and the power-base energy storage is controlled by the DC/DC converter for power exchange and then connected to the DC side of the AC-DC-AC inverter.

When the system is in a charging starting state or charging operating state, the machine side inverter is given a pulse signal, and the reference speed can be given directly at this time because the FOC control strategy is used for squirrel cage motor control. The reference speed is given as the nominal speed to ensure that the motor runs in optimal working condition.

When the system is in the discharge starting state or charging operating state, the machine side inverter is given a pulse signal, and the reference speed is specified as the negative rated speed. Then the motor reverses and operates in the discharging state.

When the system is in a charging breaking state or discharging braking state, the reference speed can be directly given to zero by FOC control, and the motor brakes when the actual speed drops to zero and stops giving pulse signals. Since the inverter itself consists of switching devices, the system is spontaneously off-grid when the inverter is turned off.

Overall, the control strategy at the distribution grid level can be organized as table 3 for the logic decision system in Fig. 12. Where BS indicates the braking signal, -1 when there is no braking (normal operation), and 1 when braking; PS indicates the machine side inverter pulse signal.

Table.3 Control logic table for transmission grid-level HGES

System Status	BS	PS	n reference
CS ($\|n\| > \|n_s\|$)	-1	1	n_N
CO	-1	1	n_N
CB ($V = 0$)	-1→(1)	1→(-1)	0
DS ($\|n\| > \|n_s\|$)	-1	1	$-n_N$
DO	-1	1	$-n_N$
DB ($V = 0$)	-1→(1)	1→(-1)	0

From the control point of view, the two different hybrid gravity storage systems which are applied to the distribution and transmission grids, the hybrid gravity storage system at the transmission grid level becomes complex to control at the equipment level but simpler at the system level due to the addition of power electronics which makes the equipment more controllable.

7 Simulation verification

This chapter is based on MATLAB/Simulink to simulate and verify the proposed HGES, including the feasibility of the system architecture of two HGES at the distribution grid level and transmission grid level, the control strategy of power electronics, the control strategy of power-based energy storage and the control strategy at the hybrid system level.

7.1. Distribution grid-level HGES

Based on the blue part in Fig. 12, a distribution grid-level HGES simulation model is established. The model parameters are shown in Table 4, and the simulation results are shown in Fig. 13. In order to present the entire process of HGES operation in a shorter time scale, the simulation time is set to 50 seconds (the operation time should be longer in reality), in which the first 25 seconds the system is charged and the last 25 seconds the system is discharged. The rated speed of the mass module is 0.2 meters per second, and the total vertical height movement is set to 4 meters (which should be much more prominent in reality). Due to the application for distribution grid level, a wound asynchronous motor with a rated capacity of 15kW is used.

628 **Table.4 Simulation parameter table for distribution grid-level HGES**

Systems	Items	Parameters
Mechanical System	Mass	1.6 t
	Height of operation	4 m
	Rated operating velocity	0.2 m/s
Motor System	Rated capacity	15 kW
	Stator resistance	0.2147 Ω
	Stator inductance	0.000991 H
	Rotor resistance	0.2205 Ω
	Rotor inductance	0.000991 H
	Mutual inductance	0.06419 H
	Inertia	0.102 $kg*m^2$
	Friction coefficient	0.009541 $N*m*s$
	Number of pole pairs	2
	Rated frequency	50 HZ
	Rated voltage	0.4 kV
	Starting resistance	3 Ω
	Braking resistance	8.25 Ω
Power-based ES	System capacity	1 F
(Supercapacitor)	Unit rated voltage	2.7 V
	Number of units	100
	System Rated Voltage	270 V
	Initial Voltage	191 V
Electric Drive system	DC/DC Inductor	0.01 H
	Voltage stabilizing capacitor	0.019 F
	Switching device on-resistance	0.001 Ω
	Switching device blocking resistance	100000 Ω
	PWM frequency	10 kHz

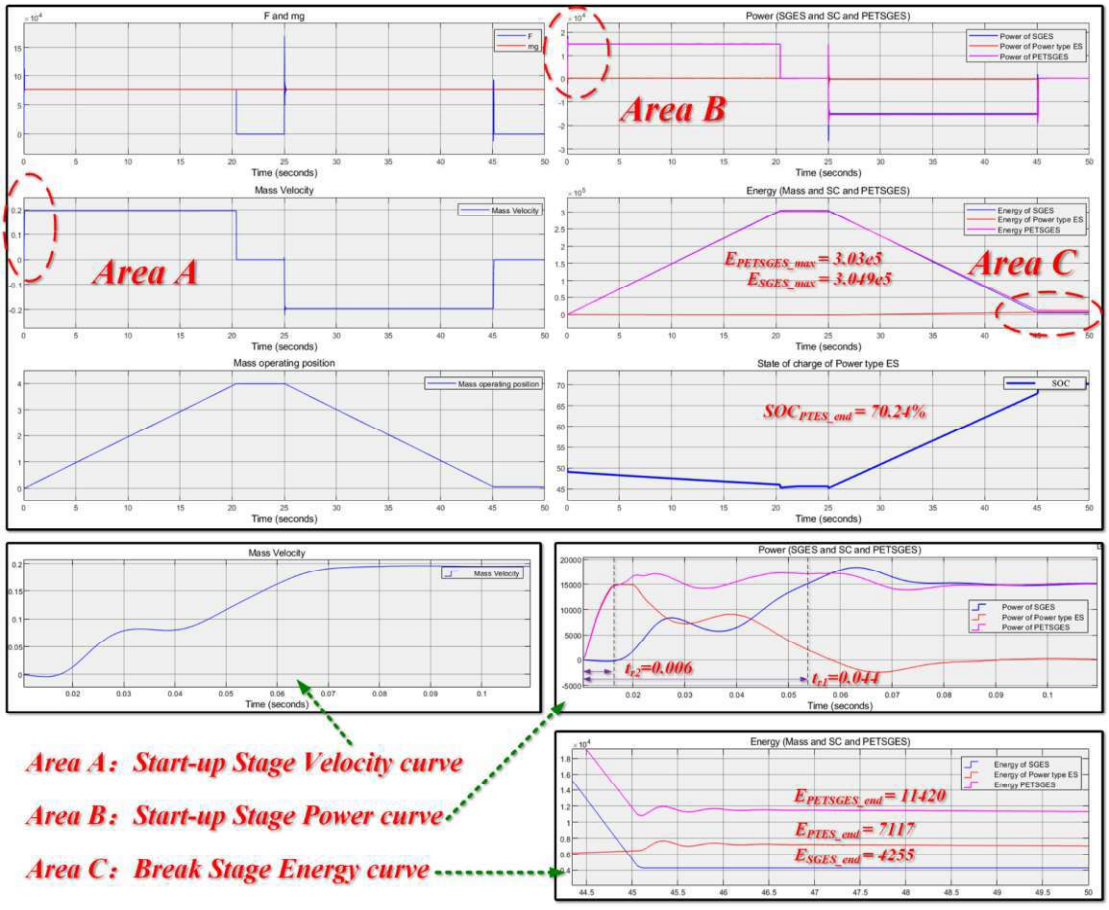

Fig. 13. Simulation results of distribution grid-level HGES system states with typical operating conditions

The left column, from top to bottom, shows the mass module's traction force and gravity, the mass module's speed, the operating position of the mass module, and the speed curve of the start-up phase. The right column from top to bottom shows the exchanged power and stored energy of the mass module, power storage, and hybrid gravity storage system; the charge state of the power-based energy storage; the power curve of the start-up phase; and the energy gain/loss curve of the system after one operating cycle.

Due to using a 15 kW motor with small electromechanical inertia, reflected in the fast nonlinear transition process of the traction force curve in the figure, the velocity and position curve of the mass module can be considered linear on a time scale of seconds. Due to the access to the negative sequence three-phase power supply in the discharge state, large but quickly decaying tractive force fluctuations exist at the instant of discharging initiation (t=25). Due to the slip rate, the motor cannot run precisely at the best operating point under the same load in both charging and discharging states. In order to ensure accurate output power, the power-based energy storage, in this case, also has a small compensating power in the stable operation stage.

The start-up stage power response curve (region B) shows that the full power response time of the hybrid gravity storage system is six milliseconds, while the original gravity storage system is 44 milliseconds. That is, the full power response speed of the hybrid energy storage system is seven times higher than the original gravity storage system under the current distribution grid simulation case.

Define the cycle efficiency of the energy storage system η_{sys} as follows:

$$\eta_{sys} = \eta_{in}\eta_{out} \tag{38}$$

Where η_{in} is the energy storage system storage efficiency; η_{out} is the energy storage system release efficiency. In particular, when the storage and release of the energy storage system have the same process, the two process efficiencies can be considered equal, then the cycle efficiency η_{sys} of the energy storage system can be written as:

$$\eta_{sys} = \left(\frac{E_0 - E_{loss}}{E_0}\right)^2 \tag{39}$$

Where E_0 is the original stored energy of the energy storage system; E_{loss} is the energy loss when releasing energy to the outside. The power-based energy storage in this simulation case uses a supercapacitor of size 1 F and rated voltage 270 V, and its stored energy can be expressed as:

$$E_{SC} = \frac{1}{2}CU^2 \tag{40}$$

Where C is the capacitance value of the supercapacitor; U is the voltage of the supercapacitor. Combining Eq. (39) and Eq. (40) with the simulation result, the efficiency of the GES system, in this case, is 97.23%, and the efficiency of the power-based energy storage system is 96.45%. The efficiency of HGES is the average of both weighted by the proportion of energy exchange, considering that the energy exchange of the GES part is much larger than that of power-based energy storage, so the efficiency of HGES should be close to 97%.

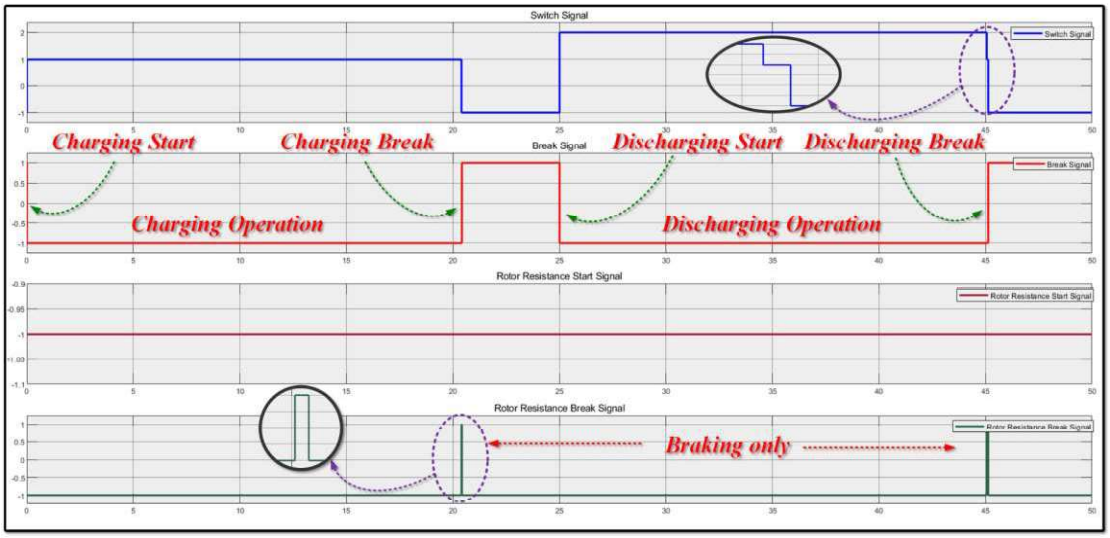

Fig. 14. Simulation results of distribution grid-level HGES system control signals with typical operating conditions

The control signal of the HGES at the distribution grid level is shown in Fig. 14, and the simulation results are consistent with those in Table 2. Since the motor capacity used is small (15kW) for small-scale distribution grid applications, there is no need to add a series starting resistor to assist in starting, and the rotor starting resistor control signal is kept at -1 (i.e., no starting resistor is used). Due to the low rotational inertia of the motor, the rotor braking resistor completes the motor's braking soon after it is connected and then cut off.

7.2. Transmission grid-level HGES

The simulation model of the transmission grid-level HGES is established based on the green part in Fig. 12, the model parameters are shown in Table 5, and the simulation results are shown in Fig. 14. Similarly, the simulation time is set to 50 seconds, in which the first 25 seconds the system is charged and the next 25 seconds the system is discharged. Considering that an enormous height difference is more

likely to be used for GES at the transmission grid level, the rated speed of the mass module is 0.5 meters per second, and the total vertical height displacement is set to 8 m (limited by the simulation duration, which should be much more prominent in reality). Due to facing the transmission grid level application, a squirrel-cage asynchronous motor with a rated capacity of 160 kW is used.

Table.5 Simulation parameter table for transmission grid-level HGES

Systems	Items	Parameters
Mechanical System	Mass	16.3 t
	Height of operation	8 m
	Rated operating velocity	0.5 m/s
Motor System	Rated capacity	160 kW
	Stator resistance	0.01379 Ω
	Stator inductance	0.000152 H
	Rotor resistance	0.007728 Ω
	Rotor inductance	0.000152 H
	Mutual inductance	0.00769 H
	Inertia	2.9 $kg * m^2$
	Friction coefficient	0.05658 $N * m * s$
	Number of pole pairs	2
	Rated frequency	50 Hz
	Rated voltage	0.4 kV
Power-based ES	System capacity	30 F
(Supercapacitor)	Unit rated voltage	2.7 V
	Number of units	600
	System Rated Voltage	1620 V
	Initial Voltage	1145 V
Electric Drive system	DC/DC Inductor	0.01 H
	Voltage stabilizing capacitor	0.019 F
	Switching device on-resistance	1e-3 Ω
	Switching device blocking resistance	1e5 Ω
	PWM frequency	10 kHz

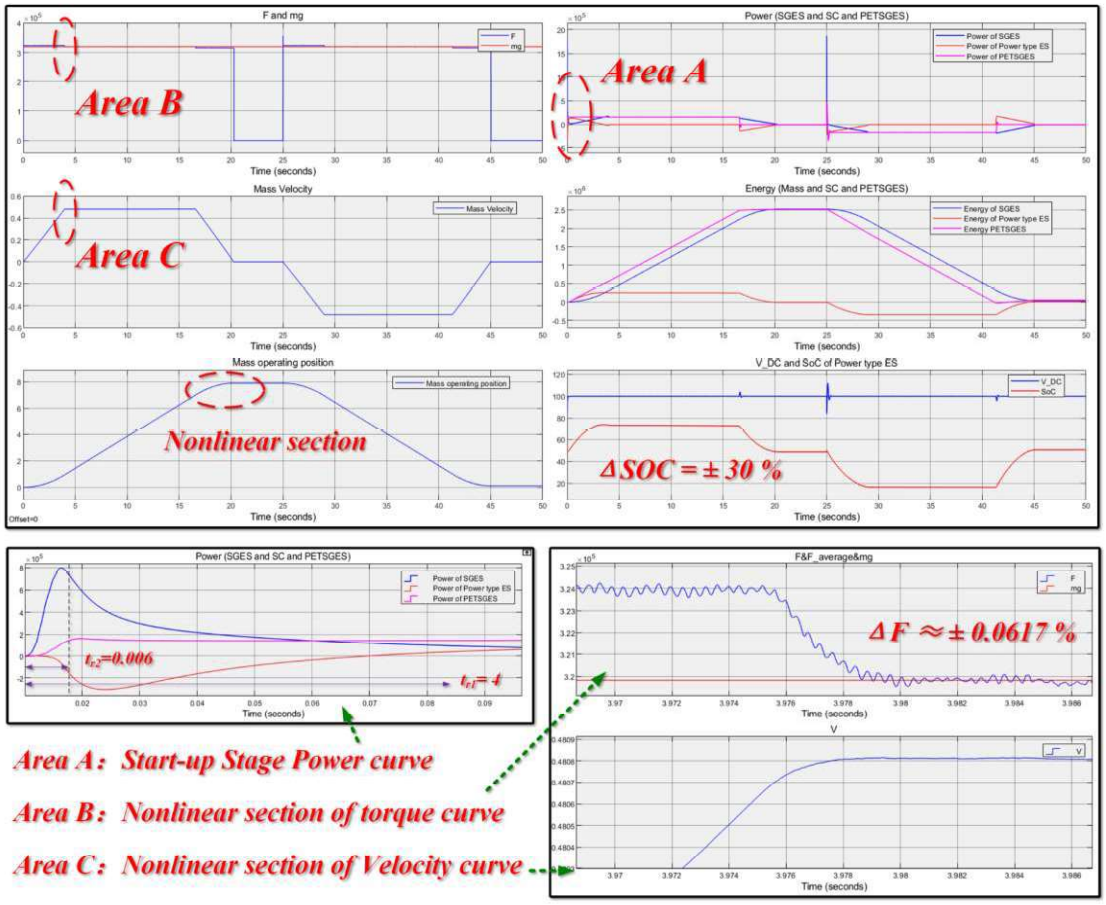

Fig. 15. Simulation results of transmission grid-level HGES system states with typical operating conditions

The layout of Fig. 15 is essentially similar to that of Fig. 13, with the image in the second column of the third row additionally containing the percentages of the DC side voltage of the AC-DC-AC inverter. Comparing the images in the left column related to the operation of the mass module, we can see that the gravity storage for larger scale applications has a more pronounced nonlinear segment of the curve due to the use of a larger capacity motor (160kW vs. 15kW) with a heavier weight (32 tons vs. 7 tons), in line with the theoretical expectations of the fourth chapter section. It should be noted that the amplified torque curve also has small, fast fluctuations in addition to the nonlinear segment. Due to the current hysteresis control strategy, this high-frequency fluctuation is tiny and will be filtered out after going through the other inertial loops of the system.

Moreover, in this case, the rectangular-based compensation method and its power-based energy storage capacity configuration strategy are based on Eqs. (36) and (40) with a 20% capacity margin (taking into account power pulses from motor start-up or for fast power fluctuation smoothing, emergency inertia support, etc.) are validated, and the capacity configuration is derived from Eq. (41):

$$C = 2\frac{t_{ramp}P_N - mV_N^2}{U_N^2(1-2\gamma)} \tag{41}$$

where t_{ramp} is the climb time of the motor speed (or mass module speed); P_N is the rated power of the compensated GES system; m is the mass of the mass module; V_N is the rated operating speed of the mass module; U_N is the rated voltage of the supercapacitor; γ is the stability margin expressed as a percentage. According to the designed capacity configuration, the SOC fluctuation of the actual power-based energy storage is limited to 30%, leaving a stability margin of 20%.

Due to the large capacity of the motor (160 kW), the rotating inertia is more considerable, and to avoid excessive temperature rise due to overcurrent during the start-up stage. In this case, the motor start-up time is set to 4 seconds, i.e., the full power response time of the gravimetric energy storage part is 4 seconds. Since the response time of power-based energy storage is in the millisecond range, the full power response time of the hybrid energy storage system after combining power-based energy storage is shortened to 6 milliseconds (similar to the application at the distribution grid level), which is a significant performance improvement with a response speed of about 670 times compared to the original GES system.

Similarly, the efficiency of the simulated gravity storage part under the transmission grid level case is 98.63%, which is an improvement compared to 97.32% at the distribution grid level, as motor efficiency generally rises with increasing capacity. Since the motor runs at the optimal operating point based on FOC control, the output is the required rated power, so the power-based energy storage device does not need to be compensated for stable operation. As a result, the energy exchange of the gravity storage part becomes the absolute main body of the hybrid gravity storage system, so the efficiency of the hybrid gravity storage system should also be close to 98%.

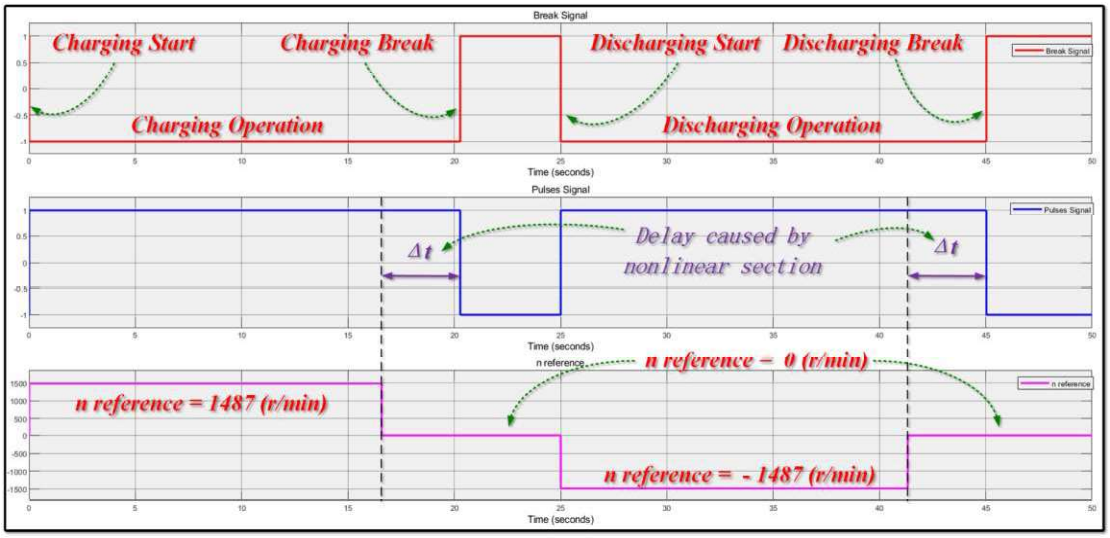

Fig. 16. Simulation results of transmission grid-level HGES system control signals with typical operating conditions

The control signal of the HGES at the transmission grid level is shown in Fig. 16, and the simulation results are consistent with those in Table 3. Due to the larger motor capacity (160kW) used for larger-scale transmission grid applications with higher rotational inertia, there is a more pronounced nonlinear segment, and this transient process leads to a delay between the pulse signal and the speed reference command.

7.3. Discussion

In both simulation cases, the HGES's efficiency is approximately equal to the GES's efficiency due to the system's overall volume of energy exchange. The simulation results show that the cycle efficiency of the GES is about 97%, which should be close to the square of the motor efficiency used - this is obviously higher than the real situation - because this simulation case does not consider the energy loss in the mechanical part of the GES. In fact, according to the HGES energy flow model shown in Fig. 5, the losses of the GES system are mainly from the motor and mechanical losses, considering that the power electronics are often very efficient. Therefore, the cycle efficiency obtained from this simulation

should be considered as the theoretical limit of the HGES cycle efficiency rather than the actual value.

The reason for not considering the mechanical system losses is that the GES system studied in this paper is an abstraction of various GES technologies (as shown in Fig. 2) and is the study of its most essential model. In contrast, the mechanical systems used in different GES technologies vary and cannot be generalized, so they are not considered in this study. The advantage of doing so is to ensure the generality of this study, which makes this study suitable for any GES technologies. If the actual efficiency of GES technologies is needed, only the efficiency of the corresponding mechanical system needs to be considered further.

From the energy perspective, another interesting phenomenon can be found in the study of HGES - under the rectangle-based compensation strategy, the energy of the hybrid energy storage system is time-shifted compared to the original GES system after the compensation of power-based energy storage. In fact, this is the very nature of energy storage systems - to decouple energy in space-time coordinates so that energy can be used in any time and space, thus achieving great flexibility.

Taking the hybrid gravity storage system as an example, we can find that the addition of power-based energy storage makes the energy of the hybrid system move on the time scale, while part of the transferred energy is transferred over space with power-based energy storage (in this case, supercapacitor) as the carrier. The power-based energy storage, as the energy storage in the storage system, optimizes the energy flow within the hybrid storage system, as the hybrid gravity storage system acts in the utility grid at a more macro-scale.

8 Conclusion

GES technology is a promising new large-scale energy storage technology, similar to pumped hydro storage, a typical energy-based energy storage technology. Combined with power-based energy storage technology, this paper proposes a hybrid GES technology based on the slow response of GES technology and the problem of significant output power fluctuation when loading and offloading heavy objects.

In this paper, we first analyze all possible structures of HGES and propose two appropriate HGES structures for distribution and transmission grid application scenarios. After obtaining a reasonable system structure, we analyze the control strategies of different structure schemes in detail according to three levels: device, single energy storage system, and hybrid energy storage system, including the power electronic control strategy at the bottom level, the control strategy of power-based energy storage, the control strategy of GES, and the overall control strategy of the hybrid system. In particular, three complementary capacity configuration schemes are also given for power-based energy storage in addition to the three basic control strategies. Finally, the simulated verification of the proposed hybrid energy storage system and its control strategy is completed based on MATLAB/Simulink platform.

The case simulation results of this study can be summarized as follows.

- The operation of the proposed HGES meets the theoretical expectations and verifies the feasibility of the proposed system structure approach, control strategy, and power-based energy storage configuration scheme.
- The power-based energy storage in the hybrid gravity storage system can well suppress the inherent power fluctuation problem of GES under the rectangular-based compensation strategy.
- The response speed of the HGES is improved by 1 to 2 orders of magnitude compared to the single GES system.
- The HGES can achieve more significant performance improvements in large-scale application

scenarios oriented to the transmission grid level.

- The efficiency of the HGES will reach more than 95% without considering the mechanical system losses, and even considering the mechanical system losses, the HGES efficiency still promises to exceed 80% with a high-efficiency mechanical system.

The proposed hybrid GES combines the large storage capacity of energy-based energy storage (MW level and above) with the high response speed of power-based energy storage (ms level). It is an ideal energy storage system without obvious performance drawbacks and will be expected to provide critical technical support for developing renewable energy power systems.

Data availability

The data that support the plots within this paper and other findings of this study are available from the corresponding author upon reasonable request.

Code availability

The code is available from the corresponding author upon reasonable request.

Reference

[1] K. M. Tan, T. S. Babu, V. K. Ramachandaramurthy, P. Kasinathan, S. G. Solanki, S. K. Raveendran. Empowering smart grid: A comprehensive review of energy storage technology and application with renewable energy integration. JOURNAL OF ENERGY STORAGE. 2021;39.

[2] M. C. Argyrou, P. Christodoulides, S. A. Kalogirou. Energy storage for electricity generation and related processes: Technologies appraisal and grid scale applications. RENEWABLE & SUSTAINABLE ENERGY REVIEWS. 2018;94:804-21.

[3] T. Kousksou, P. Bruel, A. Jamil, T. El Rhafiki, Y. Zeraouli. Energy storage: Applications and challenges. SOLAR ENERGY MATERIALS AND SOLAR CELLS. 2014;120:59-80.

[4] O. Palizban, K. Kauhaniemi. Energy storage systems in modern grids—Matrix of technologies and applications. Journal of Energy Storage. 2016;6:248-59.

[5] S. Vazquez, S. M. Lukic, E. Galvan, L. G. Franquelo, J. M. Carrasco. Energy Storage Systems for Transport and Grid Applications. IEEE Transactions on Industrial Electronics. 2010;57:3881-95.

[6] D. Parra, M. Swierczynski, D. I. Stroe, S. A. Norman, A. Abdon, J. Worlitschek, et al. An interdisciplinary review of energy storage for communities: Challenges and perspectives. RENEWABLE & SUSTAINABLE ENERGY REVIEWS. 2017;79:730-49.

[7] L. Olatomiwa, S. Mekhilef, M. S. Ismail, M. Moghavvemi. Energy management strategies in hybrid renewable energy systems: A review. RENEWABLE & SUSTAINABLE ENERGY REVIEWS. 2016;62:821-35.

[8] A. Evans, V. Strezov, T. J. Evans. Assessment of utility energy storage options for increased renewable energy penetration. RENEWABLE & SUSTAINABLE ENERGY REVIEWS. 2012;16:4141-7.

[9] W. Tong, Z. Lu, W. Chen, M. Han, G. Zhao, X. Wang, et al. Solid gravity energy storage: A review. Journal of Energy Storage. 2022;53:105226.

[10] W. Tong, Z. Lu, J. Sun, G. Zhao, M. Han, J. Xu. Solid gravity energy storage technology: Classification and comparison. Energy Reports. 2022;8:926-34.

[11] A. H. Fathima, K. Palanisamy. Optimization in microgrids with hybrid energy systems - A review. RENEWABLE & SUSTAINABLE ENERGY REVIEWS. 2015;45:431-46.

[12] J. Lian, Y. Zhang, C. Ma, Y. Yang, E. Chaima. A review on recent sizing methodologies of hybrid renewable energy systems. ENERGY CONVERSION AND MANAGEMENT. 2019;199.

[13] S. Rehman, L. M. Al-Hadhrami, M. M. Alam. Pumped hydro energy storage system: A technological review. Renewable and Sustainable Energy Reviews. 2015;44:586-98.

[14] A. Benato, A. Stoppato. Pumped Thermal Electricity Storage: A technology overview. Thermal Science and Engineering Progress. 2018;6:301-15.

[15] W. Zhang, J. Lu, Z. Guo. Challenges and future perspectives on sodium and potassium ion batteries for grid-scale energy storage. Materials Today. 2021;50:400-17.

[16] C. Zhang, X. Li. Perspective on organic flow batteries for large-scale energy storage. Current Opinion in Electrochemistry. 2021;30:100836.

[17] Y. Qiu, F. Jiang. A review on passive and active strategies of enhancing the safety of lithium-ion batteries. International

Journal of Heat and Mass Transfer. 2022;184:122288.
[18] W. Cao, B. Lei, Y. Shi, T. Dong, P. Peng, Y. Zheng, et al. Ponderation over the recent safety accidents of lithium-ion battery energy storage stations in South Korea, Energy Storage Science and Technology (2020) 1539–1547.
[19] Q. Zhou, D. Du, C. Lu, Q. He, W. Liu. A review of thermal energy storage in compressed air energy storage system. Energy. 2019;188:115993.
[20] A. G. Olabi, T. Wilberforce, M. Ramadan, M. A. Abdelkareem, A. H. Alami. Compressed air energy storage systems: Components and operating parameters – A review. Journal of Energy Storage. 2021;34:102000.
[21] M. Budt, D. Wolf, R. Span, J. Yan. A review on compressed air energy storage: Basic principles, past milestones and recent developments. Applied Energy. 2016;170:250-68.
[22] O. S. S. L. I. Consultants. Levelised Cost of Storage The Case of Gravity Storage. 2017.
[23] A. Berrada, K. Loudiyi. Chapter 7 - Conclusion. In: Berrada A, Loudiyi K, editors. Gravity Energy Storage: Elsevier; 2019. p. 163-5.
[24] A. Fyke. The Fall and Rise of Gravity Storage Technologies. Joule. 2019;3:625-30.
[25] T. Morstyn, M. Chilcott, M. D. McCulloch. Gravity energy storage with suspended weights for abandoned mine shafts. Applied Energy. 2019;239:201-6.
[26] A. Emrani, A. Berrada, M. Bakhouya. Optimal sizing and deployment of gravity energy storage system in hybrid PV-Wind power plant. Renewable Energy. 2021;183:12-27.
[27] A. Berrada, K. Loudiyi, I. Zorkani. Toward an Improvement of Gravity Energy Storage Using Compressed Air. Energy Procedia. 2017;134:855-64.
[28] A. Emrani, A. Berrada, M. Bakhouya. Modeling and Performance Evaluation of the Dynamic Behavior of Gravity Energy Storage with a Wire Rope Hoisting System. Journal of Energy Storage. 2021;33:102154.
[29] ARES. Advanced Rail Energy Storage.
[30] J. D. Hunt, B. Zakeri, G. Falchetta, A. Nascimento, Y. Wada, K. Riahi. Mountain Gravity Energy Storage: A new solution for closing the gap between existing short- and long-term storage technologies. Energy. 2019;190:116419.
[31] C. D. Botha, M. J. Kamper. Linear Electric Machine-Based Gravity Energy Storage for Wind Farm Integration. In: Botha CD, Kamper MJ, editors. 2020 International SAUPEC/RobMech/PRASA Conference2020. p. 1-6.
[32] K. R. Vasudevan, V. K. Ramachandaramurthy, G. Venugopal, J. B. Ekanayake, S. K. Tiong. Variable speed pumped hydro storage: A review of converters, controls and energy management strategies. RENEWABLE & SUSTAINABLE ENERGY REVIEWS. 2021;135.
[33] M. Han, X. Chang, J. Qing, G. Yang, T. Shang. Upper pool and lower reservoir circulation, green hills often in-pumping storage technology application and development. Science And Technology Review. 2016;34:57-67.
[34] D. Zhang, T. Chen, Y. Li, G. Liu, J. Mu, S. Lin. Study on the role of Japanese pumped storage power station in power grid. Power Technology. 2010;19:15-9.
[35] F. Li. Research on Key Technologies of Modular Multilevel Matrix Converter [D]: Shandong University; 2016.
[36] Y. Sun. Research on Modulation Strategy of Modular Multilevel Matrix Converter [M]: North China Electric Power University (Beijing); 2017.
[37] F. Li, G. Wang, R. Liu. Low Frequency Control Method of Modular Multilevel Matrix Converter. Power System Automation. 2016;40:127-33.
[38] A. Berrada, K. Loudiyi, I. Zorkani. Profitability, risk, and financial modeling of energy storage in residential and large scale applications. Energy. 2017;119:94-109.
[39] C. D. Botha, M. J. Kamper, R. J. Wang. Design optimisation and cost analysis of linear vernier electric machine-based gravity energy storage systems. Journal of Energy Storage. 2021;44:103397.
[40] Y. Y. Yi Ruan, Boshi Chen. electric drive automatic control system. 5 ed. Beijing: Mechanical Industry Press; 2016.
[41] M. N. Bin Wu. High-Power Converters and AC Drives. 2 ed: Mechanical Industry Press; 2019.
[42] X. Huang, X. Zhang, T. Wei, Z. Qi, Y. Ma. Development and Application of Supercapacitors. New Technology of Electrical Energy. 2017;36:63-70.
[43] R. T. Yadlapalli, R. R. Alla, R. Kandipati, A. Kotapati. Super capacitors for energy storage: Progress, applications and challenges. Journal of Energy Storage. 2022;49:104194.
[44] M. u. d. Mufti, S. A. Lone, S. J. Iqbal, M. Ahmad, M. Ismail. Supercapacitor based energy storage system for improved load frequency control. Electric Power Systems Research. 2009;79:226-33.

Competing interests

The authors declare no competing interests.

Acknowledgements

We would like to thank Prof. Janzhong Xu and Prof. Yanbo Chen for providing valuable comments for this paper. Funding from the State Grid Co., Ltd. Headquarters Management Science and Technology Project. Project title: “Research on the key technology of grid-connected vertical matrix-type gravity energy storage system for new power systems”. Funding number: 4000-202318089A-1-1-ZN.

Author contributions

Wenxuan Tong: led the manuscript writing; Conceptualization; Data curation; Bibliography and Analysis; Formula derivation; Investigation; Methodology; Simulation Modeling; Simulation Analysis; Manuscript Writing; Review & editing.

Zhengang Lu: Conceptualization; Formal analysis; Investigation; Methodology; Supervision; Validation; Manuscript Writing; Review & editing.

Haisen Zhao: Formal analysis; Supervision; Validation; Simulation Analysis; Review & editing.

Minxiao Han: Formal analysis; Validation; Review & editing.

Guoliang Zhao: Supervision; Validation; Review & editing.

Julian David Hunt: Manuscript revision; Review & editing.

All authors contributed to the manuscript.

Additional information

Correspondence and requests for materials should be addressed to Zhengang Lu.